



Short communication

Impregnated nickel anodes for reduced-temperature solid oxide fuel cells based on thin electrolytes of doped LaGaO₃

Xuejiao Liu, Xie Meng, Da Han, Hao Wu, Fanrong Zeng, Zhongliang Zhan*

CAS Key Laboratory of Materials for Energy Conversion, Shanghai Institute of Ceramics, Chinese Academy of Sciences (SICCAS), 1295 Dingxi Road, Shanghai 200050, China

H I G H L I G H T S

- Dual-scale porous Ni–LSGM composites are fabricated using impregnation method.
- Low ASR values of 0.011 $\Omega \text{ cm}^2$ are obtained at 550 °C for the Ni–LSGM composite anodes.
- Power densities of 1.05 W cm^{-2} are obtained at 550 °C for LSGM–electrolyte fuel cells.

A R T I C L E I N F O

Article history:

Received 6 July 2012

Received in revised form

2 August 2012

Accepted 6 August 2012

Available online 1 September 2012

Keywords:

Nickel anode

Impregnation

Nanostructure

Reduced-temperature solid oxide fuel cells

Strontium- and magnesium-doped

lanthanum gallate

A B S T R A C T

Highly active Ni-cermet anodes for thin La_{0.9}Sr_{0.1}Ga_{0.8}Sr_{0.2}O_{3-δ} (LSGM) electrolyte solid oxide fuel cells are fabricated by impregnating aqueous nickel nitrate solutions into porous LSGM backbones, followed by calcinations at 700 °C. High Ni loadings, e.g., $V_{\text{Ni}} = 7.9\%$, are mandatory for obtaining well-interconnected Ni coatings on the internal surfaces of the supporting LSGM structures, where good chemical compatibility is confirmed by the X-Ray diffraction patterns. The polarization resistances are impressively low for the $V_{\text{Ni}} = 7.9\%$ anodes in humidified hydrogen, ranging from 0.008 $\Omega \text{ cm}^2$ at 650 °C to 0.011 $\Omega \text{ cm}^2$ at 550 °C. Thin LSGM electrolyte fuel cells, impregnated with Ni anodes and Sm_{0.5}Sr_{0.5}CoO_{3-δ}–Ce_{0.8}Sm_{0.2}O_{1.9} (SSC – SDC) cathodes, exhibit superior power densities at reduced temperatures, e.g., 1.60 and 1.05 W cm^{-2} at 650 and 550 °C, respectively.

© 2012 Elsevier B.V. All rights reserved.

1. Introduction

The solid oxide fuel cell (SOFC) is an attractive electrochemical device for efficient and clean production of electricity from fossil fuels [1]. Decreasing the operating temperature from the current regime of 700–850 °C down to 500–650 °C has been a long-standing goal in the SOFC development that can reduce materials and system cost, allow the use of inexpensive alloy interconnects, simplify the gas sealing challenge and enhance the fuel cell durability [2]. Strontium- and magnesium-doped lanthanum gallate (LSGM) has emerged as a promising electrolyte for reduced-temperature SOFCs due to its high oxide ionic conductivity, negligible electronic conductivity as well as outstanding stability over a wide oxygen partial pressure range [3,4]. For example, the oxide ionic conductivities for LSGM were typically 0.17 S cm^{-1} at 800 °C

and 0.034 S cm^{-1} at 600 °C [5], which were approximately five times larger than the commonly used SOFC electrolyte, yttrium-stabilized zirconia (YSZ). Electrolyte-supported and thick film LSGM SOFCs have been fabricated and shown excellent performance at 800 °C. Single SOFCs with 200 micron thick LSGM electrolytes exhibited maximum power densities of 1.4 W cm^{-2} at 800 °C with no obvious degradation during a 30-day durability testing [6]. Nevertheless, the fuel cell power densities were still unacceptably small at lower temperatures (e.g., 600 °C) due to large ohmic resistance losses from thick electrolytes. Decreasing the electrolyte thickness is therefore required for LSGM–electrolyte fuel cells to deliver high power densities at reduced temperatures.

Note that the area-specific resistance (ASR) for a 15 μm thick LSGM electrolyte is approximately $\approx 0.05 \Omega \text{ cm}^2$ at 600 °C [5], which is low enough to attain a targeted total ASR value of 0.3 $\Omega \text{ cm}^2$ (including the electrode polarization resistances) and yield power densities of 1 W cm^{-2} . Nonetheless, fabrication of thin LSGM electrolyte SOFCs has been challenging due to chemical reactions or atomic migration of LSGM electrolyte with adjacent

* Corresponding author. Tel./fax: +86 21 6998 7669.

E-mail addresses: zzhan@mail.sic.ac.cn, zhongliangzhan@gmail.com (Z. Zhan).

electrodes when co-fired at high-temperatures to densify the electrolyte layer. Insulating compounds such as LaNiO_3 , $\text{LaSrGa}_3\text{O}_7$ and $\text{LaSrGa}(\text{Ni})\text{O}_{4-\delta}$ formed after firing a binary powder mixture of NiO and LSGM at 1050–1400 °C [7–10]. Chemical reactions were also observed at high temperatures between LSGM and doped ceria or zirconia [7,11,12]. For typical perovskite cathodes like $\text{La}_{1-x}\text{Sr}_x\text{MnO}_{3-\delta}$ and $\text{La}_{1-x}\text{Sr}_x\text{Co}_{1-y}\text{Fe}_y\text{O}_{3-\delta}$, no major second phases were observed when co-fired with LSGM. However, interdiffusion of cations could produce less conductive compounds as the electrodes and introduce electronic conduction in the electrolyte, which inevitably influences the fuel cell power density, long-term stability as well as the system efficiency [13,14].

Huang and Goodenough showed that $\text{La}_{0.4}\text{Ce}_{0.6}\text{O}_{2-\delta}$ (LDC) exhibited an iso-La chemical activity against LSGM and could be used as a barrier layer between the LSGM electrolyte and the neighboring electrodes [15,16]. Maximum power densities as high as 1.1 W cm^{-2} were achieved at 750 °C for thin LSGM-electrolyte SOFCs with thick nickel anode supports and thin LDC barrier layers fabricated using the high temperature co-firing technique [17–19]. Nonetheless, a small amount of nickel still diffused into the LSGM electrolyte, introducing electronic conductivity within the electrolyte and thus resulting in open circuit voltage values of about 100 mV lower than the Nernst potential [17]. Additionally, the presence of the LDC barrier layer substantially increased the cell ohmic resistance and thereby limited the cell power densities at reduced temperatures [17].

Pulsed laser deposition was adopted by Yan and Ishihara to deposit the thin LSGM electrolytes, where the atomic migration or chemical reaction along the interfaces was avoided since there was no high temperature step during the fuel cell fabrication. Maximum power densities of 1.95 W cm^{-2} at 600 °C were observed for the resulting LSGM/doped ceria bi-layer electrolyte fuel cells operated on hydrogen fuels and pure oxygen oxidants [20–22]. Here we report the fabrication of dual-scale Ni-LSGM anodes by high temperature ceramic processing and low temperature solution impregnation. The composite anodes feature nanoporous Ni catalyst coatings supported on the internal surfaces of high-porosity LSGM backbones, demonstrate superior catalytic activity for hydrogen oxidation and thus produce impressively low polarization resistances at reduced temperatures.

2. Experimental

The dual-scale Ni-LSGM anode was fabricated based upon an LSGM tri-layer structure – 300 μm and 60 μm thick porous layers separated by a 15 μm thick dense layer, which was produced by laminating three tape-cast ceramic green tapes, with rice starch as the fugitive material for the two porous layers. Powders of LSGM ($5 \text{ m}^2\text{g}^{-1}$, Praxair) and rice starch were ball-milled in a weight ratio of 60:40 for 24 h with appropriate amounts of dispersant, binder, plasticizer and solvent. The resulting homogeneous slurry was then cast under the doctor blade. After drying, green LSGM-starch sheets of $\approx 90 \mu\text{m}$ thick were obtained. Similarly, green LSGM electrolyte sheets of $\approx 20 \mu\text{m}$ thick were prepared by casting LSGM slurry that was formed in the same way as in the case of LSGM-starch except that no pore former was added. Four sheets of LSGM-starch, one sheet of LSGM and one sheet of LSGM-starch were stacked and uniaxially laminated at 75 °C for 10 min under a pressure of 3000 psi, which were then co-sintered at 1450 °C for 6 h in order to densify the LSGM electrolyte layer. Nickel oxide was added into the porous LSGM backbones by impregnating a 4 M aqueous nickel nitrate solution into the porous LSGM backbones, followed by calcinations at 700 °C for 30 min. Nickel nitrates were 99% pure and purchased from Sinopharm Chemical Reagent. Multiple impregnation/firing cycles were used to introduce a sufficient amount of

nickel oxide into the LSGM backbones. The quantity of the deposited NiO catalysts was estimated by the weight difference before and after each impregnation/firing cycle. Nickel oxide was reduced to Ni metal upon exposure to hydrogen fuels.

The electrochemical properties of the dual-scale Ni-LSGM anodes were assessed on both symmetric cells and anode-supported fuel cells. For symmetric cells, Ni was impregnated into both porous LSGM layers. For anode-supported cells, the 60 μm thick porous LSGM layers were simultaneously impregnated with $\text{Sm}_{0.5}\text{Sr}_{0.5}\text{CoO}_{3-\delta}$ (SSC) and $\text{Ce}_{0.8}\text{Sm}_{0.2}\text{O}_{1.9}$ (SDC) in a weight ratio of 70/30 (SSC/SDC) as previously described, whereas the 300 μm thick porous LSGM substrates were impregnated with nickel oxide. Silver ink was painted on the electrode surface as the current collector, and silver wires were used as the voltage and current leads. The active electrode area was 0.28 cm^2 . All impedance data were obtained using an IM6 Electrochemical Workstation (ZAHNER, Germany) with an ac perturbation of 20 mV. The frequency range for impedance measurement was 0.1 Hz–100 kHz. 97% H_2 –3% H_2O was used for the measurement of the anode polarization resistance in the symmetric cells. The anode supported fuel cell was tested at temperatures from 500 °C to 650 °C with the cathode exposed to ambient air and the anode to 97% H_2 –3% H_2O at a flow rate of 100 mL min^{-1} . The cell structure was examined after testing using scanning electron microscopy (SEM) in a Hitachi S-4800-II microscope.

3. Results and discussion

The dual-scale Ni-LSGM composite anode was based upon a porous LSGM backbone that exhibited a homogeneous pore structure after burning the fugitive rice starch in the green tapes. Microstructural examination using scanning electron microscopy indicated that the LSGM backbone had an average pore size of $\approx 3 \mu\text{m}$. The apparent porosity was approximately 55%, as measured by the Archimedes' method with an immersion medium of water. A thin layer of nickel oxide was deposited on the internal surfaces of the porous LSGM backbones by impregnating an aqueous nickel nitrate solution with subsequent calcinations at 700 °C. A single impregnation/calcination cycle yielded a Ni volume loading V_{Ni} of 0.6% in the porous LSGM backbone. Fig. 1a shows an SEM micrograph of the Ni-LSGM composite anode at $V_{\text{Ni}} = 0.6\%$ after exposure to hydrogen at 650 °C, showing that the Ni coating was quite uniform on the pore walls. Fig. 1b shows a higher magnification view of the Ni coating. Obviously, most of the Ni particles were isolated from each other at such a low Ni loading. In order for the Ni-LSGM composite to function well as the fuel cell anode – catalyzing the fuel oxidation and collecting the electrical current, multiple cycles of impregnation and calcination were performed to increase the nickel loading and improve the nickel phase connectivity. Fig. 2 shows the SEM micrographs of the Ni-LSGM composite anode at $V_{\text{Ni}} = 7.9\%$ after ≈ 14 impregnation cycles that exhibit well interconnected nickel coating. Comparison of Figs. 2b and 1b indicates that the Ni particles increased from $\approx 30 \text{ nm}$ at $V_{\text{Ni}} = 0.6\%$ to $\approx 80 \text{ nm}$ at $V_{\text{Ni}} = 7.9\%$, which can be explained by the repeated calcination cycles at 700 °C that can promote the NiO agglomeration and coarsening. X-Ray diffraction patterns in Fig. 3 for the $V_{\text{Ni}} = 7.9\%$ anode showed the existence of NiO and LSGM prior to hydrogen reduction. Despite several minor unknown peaks, formation of impurities like LaNiO_3 , $\text{LaSrGa}_3\text{O}_7$ and $\text{LaSrGa}(\text{Ni})\text{O}_{4-\delta}$ can be excluded in the impregnated NiO-LSGM anodes, showing good chemical compatibility between the infiltrate catalyst coating and the LSGM backbone where the highest temperature step after infiltration was 700 °C.

The catalytic activity of the dual-scale Ni-LSGM composite anode for hydrogen oxidation was initially evaluated on the

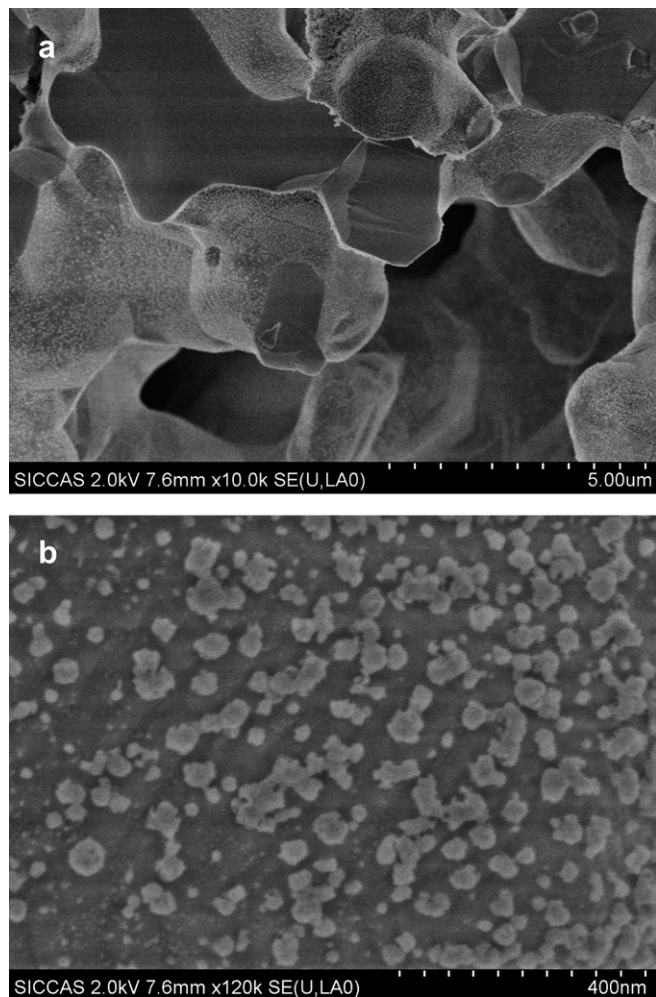


Fig. 1. The SEM micrograph of an operated Ni-LSGM anode with $V_{\text{Ni}} = 0.6\%$ at (a) low and (b) high magnification.

symmetric fuel cells: Ni-LSGM|LSGM|Ni-LSGM, where Ni was impregnated into both porous LSGM backbones. The impedance data were collected in a uniform atmosphere of 97% H_2 –3% H_2O . Fig. 4 shows the Nyquist plot of the $V_{\text{Ni}} = 7.9\%$ symmetric anode fuel cells at varied temperatures. The anode polarization resistances (R_a) correspond to the magnitude of the arcs in Fig. 4, as determined by the difference between the high- and low-frequency intercepts of the real axis. Note that the data were multiplied by 0.5 to account for two anodes. The R_a value for the $V_{\text{Ni}} = 7.9\%$ anode varied from $0.008 \Omega \text{ cm}^2$ at 650°C to $0.011 \Omega \text{ cm}^2$ at 550°C . The impressively low polarization resistances of the impregnated Ni-LSGM anodes have previously been explained by the very high density of triple-phase (Ni-LSGM-pore) boundaries in the dual micron and nano-scale porous structure [23]. The micron-scale anodes have much higher R_a values, e.g., $2.4 \Omega \text{ cm}^2$ in humidified hydrogen at 650°C for the conventional NiO-YSZ cermet prepared by sintering the their powder mixture [24]. Klemensø et al. fabricated the impregnated NiO-YSZ composite in a similar manner and reported an R_a value of $0.25 \Omega \text{ cm}^2$ in 97% H_2 –3% H_2O at 650°C , which seems to suggest that the oxide ionic conduction in the backbones critically influences the catalytic behavior of the composite anode for hydrogen oxidation reactions. Similar effect on the oxygen reduction reaction has been observed in the dual scale SSC – LSGM and SSC – YSZ cathodes [25]. The $V_{\text{Ni}} = 7.9\%$ anode polarization resistances are also lower than our previously reported R_a value of

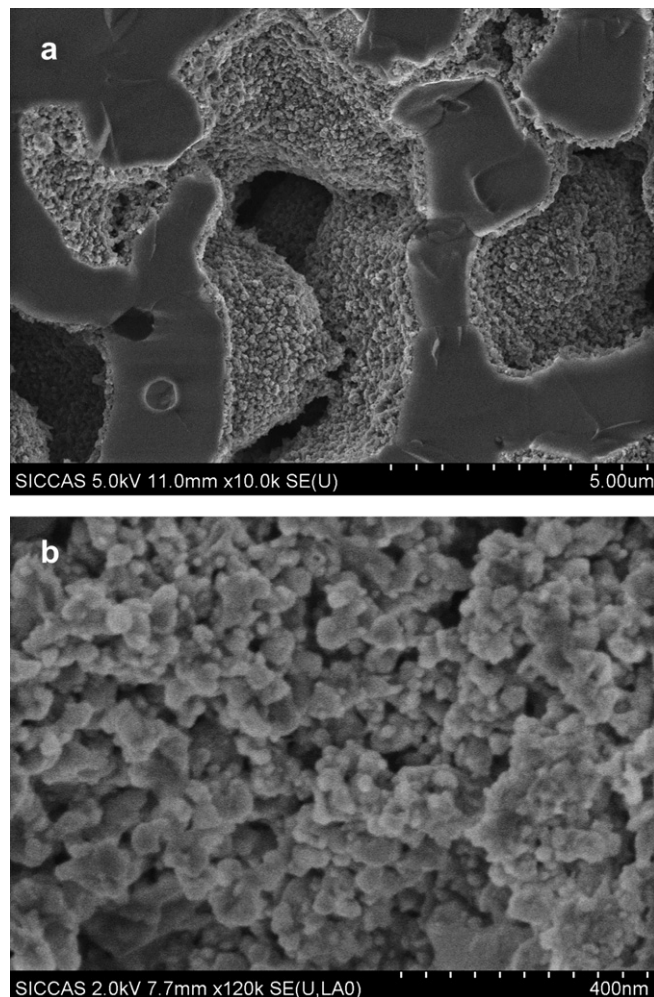


Fig. 2. The SEM micrograph of an operated Ni-LSGM anode with $V_{\text{Ni}} = 7.9\%$ at (a) low and (b) high magnification.

$0.03 \Omega \text{ cm}^2$ at 650°C for the impregnated Ni-LSGM anode at $V_{\text{Ni}} = 2.5\%$ [23]. This difference might result from different pore structures of the LSGM backbones and different measurement method, where the $V_{\text{Ni}} = 2.5\%$ anode R_a value was obtained by subtracting the cathode polarization resistance from the total

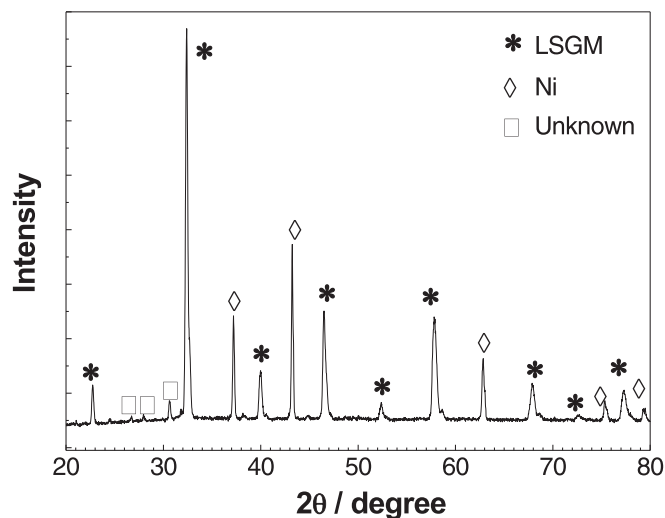


Fig. 3. XRD pattern of an NiO-LSGM composite anode with $V_{\text{Ni}} = 7.9\%$.

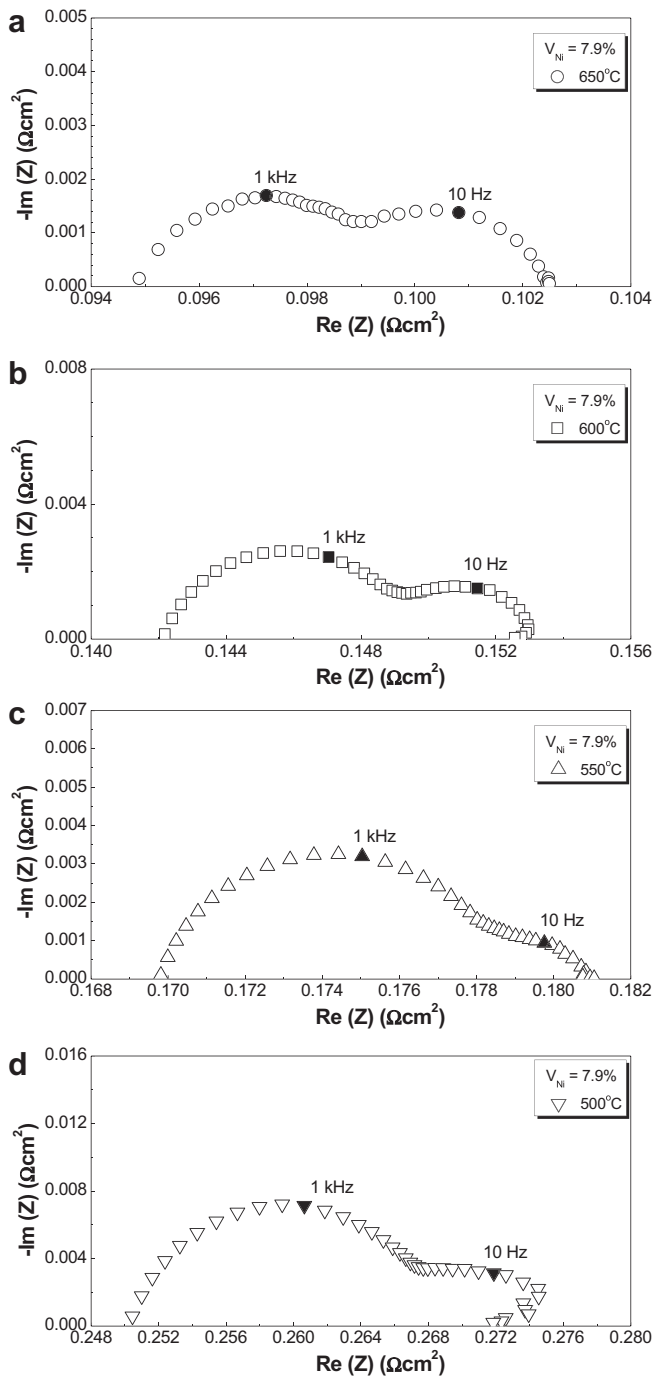


Fig. 4. Representative Nyquist plot of impedance data for symmetric anode fuel cells with $V_{\text{Ni}} = 7.9\%$ in 97% H_2 –3% H_2O at (a) 650 °C, (b) 600 °C, (c) 550 °C and (d) 500 °C.

electrode polarization resistance for an anode-supported fuel cell [23].

The R_a value for the Ni-LSGM anodes at 550 °C with varied Ni loadings are shown in Fig. 5, together with the pure ohmic resistances of the cell (R_o) obtained from the high-frequency intercepts in the Nyquist plot as shown in Fig. 4c. Notably, decreasing the Ni loading resulted in higher R_a and R_o values. For example, with the Ni loading decreasing from $V_{\text{Ni}} = 7.9\%$ to $V_{\text{Ni}} = 1.8\%$, the R_o value increased from 0.17 $\Omega\text{ cm}^2$ to 0.26 $\Omega\text{ cm}^2$, and the R_a value increased from 0.014 $\Omega\text{ cm}^2$ by a factor of 8 to 0.108 $\Omega\text{ cm}^2$. This is not surprising given that the reduced Ni phase connectivity at low Ni

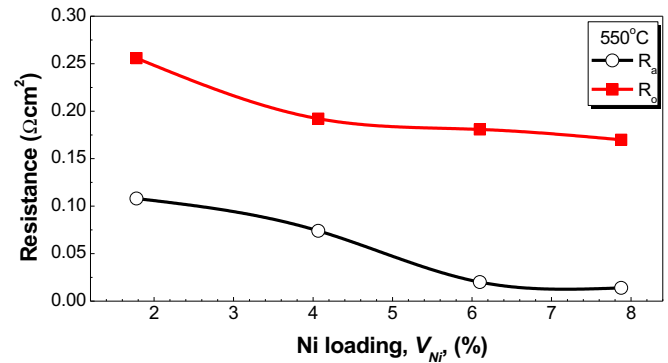


Fig. 5. Anode polarization resistance (R_a) and ohmic resistance (R_o), obtained from impedance spectra for the symmetric anode fuel cells, versus the Ni loading (V_{Ni}).

loadings, as evidenced by comparison of Figs. 1 and 2, would disable the electrochemical activity of the isolated Ni particles and decrease the electronic conductivity of the Ni-LSGM composite anodes.

The electrochemical property of the dual-scale Ni-LSGM composite anode was also evaluated on an anode-supported fuel cell: (Ni)-LSGM|LSGM|(SSC/SDC)-LSGM, where SSC/SDC in a weight ratio of 70/30 was impregnated into the thin porous LSGM layer while Ni was impregnated into the thick porous LSGM support. SSC/SDC was chosen as the active cathode component due to its high catalytic activity for oxygen reduction and low polarization resistances, e.g., 0.020 $\Omega\text{ cm}^2$ at 650 °C and 0.075 $\Omega\text{ cm}^2$ at 550 °C [26]. Fig. 6a shows the cell voltages and power densities as a function of current densities for such a fuel cell, operating on 97% H_2 –3% H_2O and ambient air at 500–650 °C. The open circuit voltages ranged from 1.10 V to 1.14 V and were in good agreement with the thermodynamically predicted Nernst potentials, indicative of good gas impermeability of the 15 μm thick LSGM electrolyte layer and elimination of atomic migration between the LSGM electrolyte and the active electrode component such as Ni and SSC/SDC. The maximum power densities were 1.60, 1.31, 1.05 and 0.73 W cm^{-2} at 650, 600, 550 and 500 °C, respectively. Fig. 6b shows the Nyquist plots of the cell impedance at open circuits that exhibited pure ohmic resistances of 0.079, 0.144, 0.187 and 0.250 $\Omega\text{ cm}^2$ as well as total area specific resistances of 0.153, 0.271, 0.368, and 0.545 $\Omega\text{ cm}^2$ at 650 °C, 600, 550 and 500 °C, respectively. Due to the extremely small polarization resistances of the anode, the cathode polarization resistances can be approximated as the magnitude of the arcs in Fig. 6b, i.e., 0.074, 0.127, 0.181 and 0.295 $\Omega\text{ cm}^2$ at 650 °C, 600, 550 and 500 °C, respectively. These polarization resistances for SSC/SDC impregnated LSGM cathodes were 2–4 times larger than previously reported values which were obtained from impedance measurement on the symmetric cathode fuel cells [26]. Note that the pure ohmic resistances in Fig. 6b were a little higher than the expected values for the 15 μm thick LSGM electrolyte, probably resulting from current collection losses in the testing setup.

The above results have shown that the dual-scale Ni-LSGM anodes are highly active for electrochemical oxidation of hydrogen. The kinetics for hydrogen oxidation in the Ni-cermet anode is governed by a number of fundamental physicochemical processes, including gas transport within the pores, adsorption and desorption of gas species on the nickel surfaces, chemical reactions of surface adsorbants as well as charge transfer reactions along the triple-phase boundaries that supply oxygen on the nickel surfaces [27]. As shown in Fig. 4, the Nyquist plots exhibited two depressed semicircles, centered at 1 kHz and 10 Hz, respectively. When decreasing the temperature from 650 °C to 550 °C, the high-frequency semicircles increased dramatically, whereas the low-

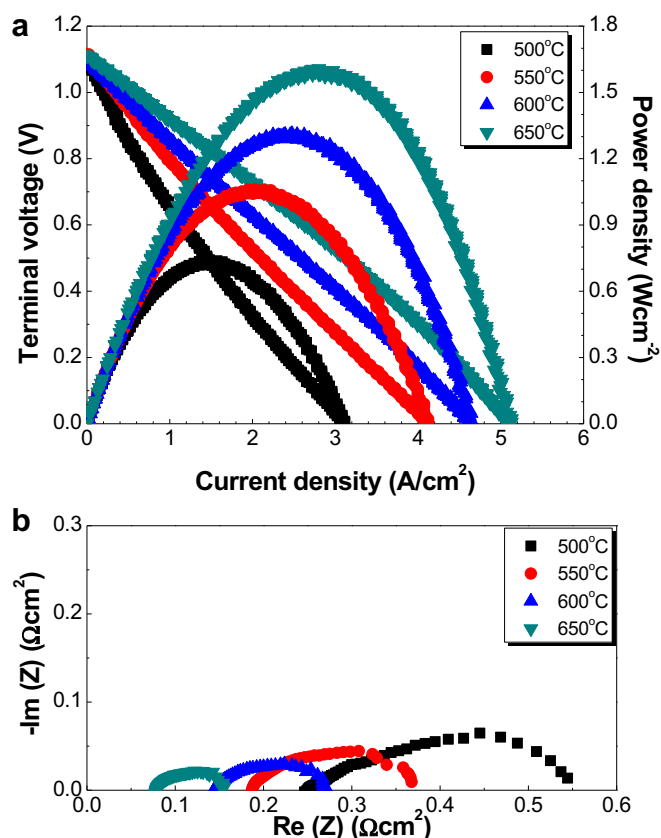


Fig. 6. (a) Voltage and power density versus current density and (b) impedance spectra for an anode-supported, thin LSGM electrolyte fuel cell with electrode loadings $V_{\text{Ni}} = 7.9\%$ and $V_{\text{SSC-SDC}} = 12.9\%$ measured in 97% H_2 –3% H_2O fuels and ambient air oxidants.

frequency semicircles remained almost unaltered. The magnitude of the high-frequency semicircles is estimated from the Nyquist plots and is summarized in Fig. 7 for the dual-scale Ni-LSGM anodes at varied Ni loadings. The activation energy decreased substantially with increasing Ni loadings. In particular, the activation energy was 1.17 eV for $V_{\text{Ni}} = 1.8\%$ and 0.62 eV for $V_{\text{Ni}} = 7.9\%$, showing different

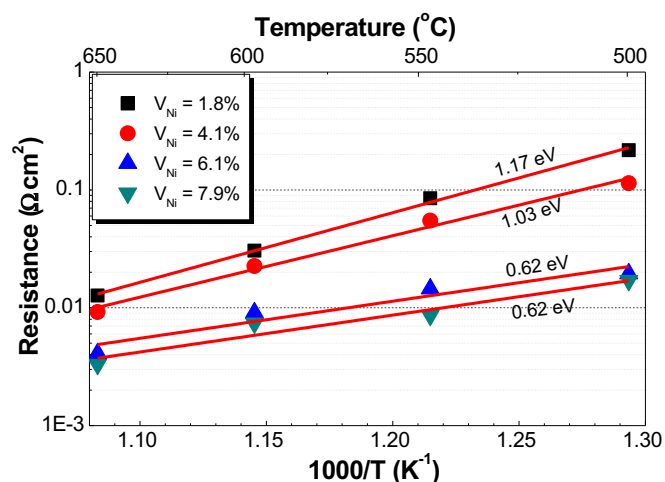


Fig. 7. The high-frequency polarization resistance for the Ni-LSGM anodes with different Ni loadings at varied temperatures, derived from the impedance data, plotted versus inverse temperature.

rate-limiting steps at these two Ni loadings. Note that more careful studies are required to get insights into hydrogen oxidation mechanism behind these electrochemical impedance spectra for symmetric anode fuel cells.

4. Conclusions

In summary, we have reported the fabrication of dual micron and nano porous Ni-LSGM composite anodes by coating a thin layer of NiO onto the internal surfaces of high-porosity LSGM backbones via impregnation and calcinations of aqueous nickel nitrate solutions. Measurement of symmetric anode fuel cells revealed unprecedentedly low polarization resistances, e.g., $0.011 \Omega \text{ cm}^2$ in 97% H_2 –3% H_2O at 550 °C, that enabled high power densities for thin LSGM electrolyte fuel cells at reduced temperatures. In particular, the maximum power densities were 1.60, 1.31, 1.05 and 0.73 W cm^{-2} at 650, 600, 550 and 500 °C, respectively.

Acknowledgements

The authors gratefully acknowledge the financial support of the National Basic Research Program of China under contract No. 2012CB215401, the National Science Foundation of China under contract No. 51072219, Science and Technology Commission of Shanghai Municipality under contract No. 09JC1415200 and 11PJ1410300, the 100 Talents Program of Chinese Academy of Sciences.

References

- [1] N.Q. Minh, J. Am. Ceram. Soc. 76 (1993) 563–588.
- [2] E.D. Wachsman, K.T. Lee, Science 334 (2011) 935–939.
- [3] M. Feng, J.B. Goodenough, Eur. J. Sol. State Inorg. 31 (1994) 663–672.
- [4] T. Ishihara, H. Matsuda, Y. Takita, J. Am. Chem. Soc. 116 (1994) 3801–3803.
- [5] X.C. Lu, J.H. Zhu, J. Electrochem. Soc. 155 (2008) B494–B503.
- [6] J.H. Wan, J.Q. Yan, J.B. Goodenough, J. Electrochem. Soc. 152 (2005) A1511–A1515.
- [7] X.G. Zhang, S. Ohara, R. Maric, H. Okawa, T. Fukui, H. Yoshida, T. Inagaki, K. Miura, Solid State Ionics 133 (2000) 153–160.
- [8] T.M. He, P.F. Guan, L.G. Cong, Y. Ji, H. Sun, J.X. Wang, J. Liu, J. Alloy Compd. 393 (2005) 292–298.
- [9] P.N. Huang, A. Horky, A. Petric, J. Am. Ceram. Soc. 82 (1999) 2402–2406.
- [10] P. Datta, P. Majewski, F. Aldinger, Mater. Chem. Phys. 102 (2007) 125–131.
- [11] M. Hrovat, A. Ahmad-Khanlou, Z. Samardzija, J. Holc, Mater. Res. Bull. 34 (1999) 2027–2034.
- [12] T.J. Armstrong, A.V. Virkar, J. Electrochem. Soc. 149 (2002) A1565–A1571.
- [13] J.Y. Yi, G.M. Choi, Solid State Ionics 148 (2002) 557–565.
- [14] D.I. Bronin, B.L. Kuzin, I.Y. Yaroslavtsev, N.M. Bogdanovich, J. Solid State Electrochem. 10 (2006) 651–658.
- [15] K. Huang, J.H. Wan, J.B. Goodenough, J. Electrochem. Soc. 148 (2001) A788–A794.
- [16] Z. Bi, M. Cheng, Y. Dong, H. Wu, Y. She, B. Yi, Solid State Ionics 176 (2005) 655–661.
- [17] Y.B. Lin, S.A. Barnett, Electrochem. Solid-State Lett. 9 (2006) A285–A288.
- [18] W.M. Guo, J. Liu, Y.H. Zhang, Electrochim. Acta 53 (2008) 4420–4427.
- [19] Z.H. Bi, B.L. Yi, Z.W. Wang, Y.L. Dong, H.J. Wu, Y.C. She, M.J. Cheng, Electrochem. Solid-State Lett. 7 (2004) A105–A107.
- [20] J.W. Yan, H. Matsumoto, M. Enoki, T. Ishihara, Electrochem. Solid-State Lett. 8 (2005) A389–A391.
- [21] T. Ishihara, J.W. Yan, M. Shinagawa, H. Matsumoto, Electrochim. Acta 52 (2006) 1645–1650.
- [22] J.W. Yan, H. Matsumoto, T. Akbay, T. Yamada, T. Ishihara, J. Power Sources 157 (2006) 714–719.
- [23] Z.L. Zhan, D.M. Bierschenk, J.S. Cronin, S.A. Barnett, Energy Environ. Sci. 4 (2011) 3951–3954.
- [24] M. Pihlatie, T. Ramos, A. Kaiser, J. Power Sources 193 (2009) 322–330.
- [25] D. Han, X.J. Liu, F.R. Zeng, J.Q. Qian, T.Z. Wu, Z.L. Zhan, Scientific Rep. 2 (2012) 462.
- [26] Z.L. Zhan, D. Han, T.Z. Wu, X.F. Ye, S.R. Wang, T.L. Wen, S. Cho, S.A. Barnett, RSC Adv. 2 (2012) 4075–4078.
- [27] W.G. Bessler, Solid State Ionics 176 (2005) 997–1011.